

13 Iron in ferropericlase experiences a spin crossover from a high spin to a low spin
14 under lower mantle conditions, which generates anomalies in many properties such as
15 the heat capacity and sound velocity. In this study, the effect of the spin crossover on
16 thermal conductivity was evaluated by considering the effects of the spin crossover on
17 P wave velocity and heat capacity at constant volume but ignoring the effect on mean
18 free path. The spin crossover completely changes the conventional pressure and
19 temperature dependences of the thermal conductivity. The spin crossover can
20 significantly reduce the thermal conductivity of ferropericlase. The pressure
21 dependence of the thermal conductivity of ferropericlase will show a double-valley
22 feature across the spin-crossover region at the appropriate temperature (e.g., 1000 K).
23 In contrast to the conventional decrease in the thermal conductivity with temperature,
24 the thermal conductivity of ferropericlase in the Earth's D'' layer may increase with
25 temperature in some temperature regions. The unusual effect of spin crossover on the
26 thermal conductivity can be expected in other minerals with spin crossover. The spin
27 crossover effect needs serious consideration when estimating the thermal conductivity
28 at the core-mantle boundary.

29 Introduction

30 Thermal conductivity of the mantle minerals is one of the key parameters that control
31 mantle convection. The heat flux from the core, which is determined by the heat
32 conductivity of the thin layer overlying the core-mantle boundary (CMB), is critical to
33 the understanding of many processes such as the Earth's evolution, mantle convection,
34 and geodynamo, while the thermal conductivity of the lower-mantle minerals at the
35 CMB is fundamental in estimating the heat flux from the core. Thus, the lattice thermal
36 conductivity of ferropericlase ($\text{Mg}_{1-x}\text{Fe}_x\text{O}$), bridgmanite and post perovskite have been
37 investigated intensively both by experiments [*Beck et al.*, 2007; *Dalton et al.*, 2013;
38 *Goncharov et al.*, 2010; *Hofmeister*, 2014; *Hsieh et al.*, 2017, 2018; *Imada et al.*,
39 2014; *Katsura*, 1997; *Manga and Jeanloz*, 1997; *Manthilake et al.*, 2011; *Ohta et al.*,
40 2014; *Ohta et al.*, 2017; *Osako and Ito*, 1991; *Okuda et al.*, 2017; *Rainey and Kavner*,
41 2014; *Hofmeister and Branlund* 2015] and theoretical calculations [*de Koker*, 2009;
42 2010; *Dekura et al.*, 2013; *Haigis et al.*, 2012; *Stackhouse et al.*, 2010; 2015; *Tang*
43 *and Dong*, 2010; *Tang et al.*, 2014; *Ghaderi et al.* 2017; *Zhang et al.*, 2017]. The
44 spin-state crossover of iron in the lower mantle minerals has been found to affect
45 significantly their elasticity, thermodynamic properties and transport properties [*Lin et*
46 *al.*, 2013]. The spin crossover may profoundly affect the lattice thermal conductivity of
47 the lower mantle. However, knowledge of the spin-crossover effect on the lattice
48 thermal conductivity is very limited. To our knowledge, first-principle calculations
49 were conducted on the Mg endmembers of ferropericlase, bridgmanite and post

50 perovskite. Only a few experiments measured the lattice thermal conductivity of
51 ferropericlae with pressures surpassing the spin-transition pressure [Hsieh *et al.*, 2018;
52 Ohta *et al.*, 2017]. Ohta *et al.* [Ohta *et al.*, 2017] observed an anomalous reduction in
53 thermal conductivity of ferropericlae in the spin crossover region. Hsieh *et al.* [2018]
54 shows that the reduction only occurs in ferropericlae with very high iron concentration.
55 The mechanism for the reduction has not been fully explored. The controversial
56 experimental results call for theoretical investigations on the effect of spin crossover on
57 the thermal conductivity.

58 The lattice thermal conductivity can be expressed as (Hofmeister and Branlund
59 2015),

$$60 \quad k_{lat} = \frac{\rho}{3ZM} C_V V_P^2 \langle \tau \rangle \quad (1)$$

61 where V_P is the compressional velocity, C_V is heat capacity at constant volume, M is
62 the molar formula weight, Z is the number of formula units in the primitive unit cell,
63 and $\langle \tau \rangle$ is the mean free lifetime. The Eq. 1 has been used to satisfactorily describe
64 the lattice thermal conductivity of several perovskites [Hofmeister, 2010]. As shown
65 in Eq. 1, k_{lat} is sensitive to the sound velocity and heat capacity. Both are extremely
66 affected by the spin crossover of iron in ferropericlae. The spin crossover causes an
67 anomalous softening in the bulk modulus and significantly reduces the V_P of
68 ferropericlae [Crowhurst *et al.*, 2008; Fei *et al.*, 2007; Komabayashi *et al.*, 2010; Lin
69 and Tsuchiya, 2008; Mao *et al.*, 2011; Marquardt *et al.*, 2009; Tsuchiya *et al.*, 2006;
70 Wentzcovitch *et al.*, 2009; Z Q Wu *et al.*, 2013; Yang *et al.*, 2015], which results in an

71 unusual positive temperature dependence of the V_P of ferropericlasite within part of the
72 spin-crossover region [Wu and Wentzcovitch, 2014]. The temperature insensitivity of
73 V_P in the mid-lower mantle caused by the opposite temperature dependence of V_P of
74 bridgmanite and ferropericlasite is consistent with the P-wave disruption in the plume
75 image below the Hawaii and Iceland hot spots at a depth of 1500–2000 km and the
76 global disruption of the faster-than-average V_P structure at the depth of ~ 1700 km
77 [van der Hilst and Karason, 1999; Wu and Wentzcovitch, 2014; Z Q Wu, 2016; Z Q
78 Wu and Wentzcovitch, 2017; Zhao, 2007]. The spin crossover of iron in ferropericlasite
79 also generates an anomaly in the thermodynamic properties of ferropericlasite such as a
80 several-fold increase in the thermal expansion and a peak in the heat capacity [Z Wu
81 et al., 2009], which controls the structural feature of the large low shear velocity
82 provinces above the CMB [Huang et al., 2015] and significantly modifies the mantle
83 flow [Bower et al., 2009; Shahnas and Peltier, 2015; Shahnas et al., 2016; Shahnas et
84 al., 2017; Shahnas et al., 2011]. Thus, we can expect that the spin crossover can
85 dramatically impact the thermal conductivity of ferropericlasite. However, its effect on
86 thermal conductivity has not yet been studied in detail.

87 **Theoretical model**

88 The Gibbs free energy of ferropericlasite in a mixed spin (MS) state, $G(n,P,T)$, is
89 given by [Z Q Wu et al., 2013]

$$90 \quad G(n,P,T) = nG_{LS}(P,T) + (1-n)G_{HS}(P,T) + G_{mix} \quad (2)$$

91 where n is the fraction of the low spin state (LS), G_{LS} and G_{HS} are the Gibbs free
 92 energies of the pure LS and HS states, respectively, and G_{mix} is the free energy of
 93 mixing of an HS/LS mixture

$$94 \quad G_{mix}(n) = -TS_{mix}(n) = k_B T X_{Fe} [n \ln n + (1-n) \ln(1-n)] \quad (3)$$

95 Here, X_{Fe} is the iron concentration in ferropicalse ($Mg_{1-X_{Fe}}Fe_{X_{Fe}}O$) and the entropy
 96 of mixing is assumed to be that of an ideal solution, which is justified by the negligible
 97 iron-iron interactions implied by the independence of the spin transition pressure on iron
 98 concentrations up to the concentration ~ 0.2 [Tsuchiya *et al.*, 2006; Persson *et al.*,
 99 2006]. The minimization of the free energy with respect to the LS fraction, n , gives

$$100 \quad n(P, T) = \frac{1}{1 + m(2S + 1) \exp \left[\frac{\Delta G_{LS-HS}^{stat+vib}}{X_{Fe} K_B T} \right]} \quad (4)$$

101 where $\Delta G_{LS-HS}^{stat+vib}$ is the difference in the Gibbs free energy from the static and
 102 vibration contribution between the HS and LS states, and $S=2$ and $m=3$ are the spin
 103 and electronic configuration (orbital) degeneracy values of the HS state, respectively.

104 Since $V(n) = nV_{LS}(P, T) + (1-n)V_{HS}(P, T)$, we have the following expression
 105 for the bulk modulus, $K(n)$,

$$106 \quad \frac{V(n)}{K(n)} = n \frac{V_{LS}}{K_{LS}} + (1-n) \frac{V_{HS}}{K_{HS}} - (V_{LS} - V_{HS}) \frac{\partial n}{\partial P} \quad (5)$$

107 where V_{HS} and V_{LS} are the volume of HS and LS, respectively, and $K_{HS/LS}$ is the
 108 bulk modulus of the pure HS/LS states. The first two terms in the right side of Eq. 5 are
 109 the weight average of those of the HS and LS states. The last terms in Eq. 5 appears

110 only at the spin-crossover region and is always positive since $\frac{\partial n}{\partial P} > 0$ and $V_{HS} > V_{LS}$.

111 Therefore, spin crossover causes an anomalous softening in the bulk modulus and
 112 reduces the compressional velocity. We defined

$$113 \quad R_{V_P^2} = \left(\frac{V_P}{V_P^{mix}} \right)^2 \quad (6)$$

114 where $V_P^{mix} = nV_P^{LS} + (1-n)V_P^{HS}$ is the weight average of the V_P of LS and HS.

115 The entropy is given by

$$116 \quad S = - \left(\frac{\partial G}{\partial T} \right)_P = nS_{LS} + (1-n)S_{HS} + (G_{HS} - G_{LS}) \left(\frac{\partial n}{\partial T} \right)_P + S_{mix}, \quad (7)$$

117 The lattice heat capacity at constant volume (C_V) and at constant pressure (C_P) is
 118 calculated from the entropy

$$119 \quad C_V = T \left(\frac{\partial S}{\partial T} \right)_V \quad (8)$$

$$120 \quad C_P = T \left(\frac{\partial S}{\partial T} \right)_P = nC_P^{LS} + (1-n)C_P^{HS} \quad (9)$$

$$+ 2T(S_{LS} - S_{HS}) \left(\frac{\partial n}{\partial T} \right)_P + T(G_{HS} - G_{LS}) \left(\frac{\partial^2 n}{\partial T^2} \right)_P + T \frac{\partial S_{mix}}{\partial T}$$

121 The contribution of the spin crossover on the heat capacity, which is described by the
 122 last three terms in Eq. 9, can be positive or negative at the spin-crossover region. We
 123 defined

$$124 \quad R_{C_V} = \frac{C_V}{C_V^{mix}}, \quad (10)$$

125 where $C_V^{mix} = nC_V^{LS} + (1-n)C_V^{HS}$ is the weight average of C_V of LS and HS.

126 We introduce $k_{latt}^{mix} = \frac{\rho}{3ZM} C_V^{mix} (V_P^{mix})^2 \langle \tau \rangle$ to approximately describe the thermal
127 conductivity of the mechanic mixture of LS and HS. The unusual effect of the spin
128 crossover on the thermal conductivity of ferroperricite can be described by

$$129 \quad R_k = \frac{k_{latt}}{k_{latt}^{mix}} = R_{V_P^2} R_{C_V} \quad (11)$$

130 Here, we ignore the effect of the spin crossover on the mean free lifetime $\langle \tau \rangle$. $\langle \tau \rangle$ of
131 MS may be smaller than the weight average of that of LS and of HS because of
132 increased scattering in MS with two types of iron. Thus, R_k probably is reduced
133 further after including the spin-crossover effect on $\langle \tau \rangle$.

134 Wu et al., have studied the effect of the spin crossover on thermodynamic
135 properties and sound velocities of ferroperricite with $X_{Fe}=0.1875$ [Z Q Wu et al.,
136 2009; 2013]. These data were used here to investigate the effect of spin crossover on
137 thermal conductivity of ferroperricite with $X_{Fe}=0.1875$. At low iron concentration
138 ($X_{Fe} < 0.2$), where $n(P,T)$ is insensitive to the X_{Fe} , the anomalous softening in bulk
139 modulus caused by spin crossover increases almost linearly with X_{Fe} (Z Q Wu et al.,
140 2013; Wu and Wentzcovitch 2017) and the last three terms in Eq. 9 also linearly
141 depend on X_{Fe} . Thus we can use the relation $1-R_{V_P^2} \propto X_{Fe}$ and $1-R_{C_V} \propto X_{Fe}$ to estimate
142 approximately the effect of the spin crossover on thermal conductivity of ferroperricite
143 with low iron concentration.

144 **Result**

145 As shown in Fig. 1a, the minimum of $R_{V_P^2}$ is ~ 0.6 at room temperature at the
146 spin-crossover region. Although the effect of the spin crossover on V_P decreases

147 with increasing temperature because of the broadening of the spin-crossover region,
148 the spin crossover can still reduce $R_{V_p^2}$ to 0.84, even at a high temperature of 4000 K.
149 With increasing temperature, the spin crossover first slightly reduces both C_V and C_P
150 and then increases significantly C_V and C_P and generates a peak value of C_V and C_P
151 around the temperature where V_P shows the minimum value (Fig. 1). Thus, in
152 contrast to $R_{V_p^2}$, which is always smaller than 1 at the spin-crossover region, R_{C_V} can
153 be larger or smaller than 1. The PT region with $R_{C_V} > 1$ overlaps well with the region
154 where $R_{V_p^2}$ is significantly smaller than 1. The regions with $R_{C_V} < 1$ surround the
155 region with $R_{C_V} > 1$. The temperature of peak value of R_{C_V} is close to that of the
156 minimum of $R_{V_p^2}$. With increasing temperature, the peak value of R_{C_V} remains almost
157 constant at ~ 1.15 , while the effect of the spin crossover on V_P decreases notably (Fig.
158 1).

159 The spin crossover causes a significant anomaly in the thermal conductivity (Fig.
160 2). At room temperature, the reduction of the thermal conductivity dominantly results
161 from the effect of the spin crossover on V_P . The effect of the spin crossover on V_P can
162 reduce the thermal conductivity of ferroperricite with $X_{Fe}=0.1875$ by $\sim 40\%$, which
163 can roughly explain the experimental results (Fig. 3). This finding suggests that the
164 unusual reduction in the thermal conductivity of ferroperricite at spin-crossover
165 pressures at room temperature reported by Ohta *et al.*[Ohta *et al.*, 2017] might mainly
166 result from the unusual effect of the spin crossover on V_P . Since $1-R_{V_p^2} \propto X_{Fe}$, the
167 spin crossover can reduce the thermal conductivity of ferroperricite with $X_{Fe} = 0.1$ by

168 roughly 20%. This value is close to the experimental uncertainty for thermal
169 conductivity [Hsieh *et al.*, 2018]. This factor coupled with the broad pressure range of
170 spin crossover makes the experimental observation of the reduction of thermal
171 conductivity challenge for ferropicicase with low iron concentration. This may
172 explain why Hsieh *et al.*, (2018) only found the clear reduction of thermal conductivity
173 in spin-crossover region for ferropicicase with $X_{Fe}= 0.56$ among three concentrations
174 $X_{Fe}=0.56, 0.1$ and 0.08 .

175 One unusual feature is that the spin crossover not only reduces the thermal
176 conductivity but also generates a negligible effect on the thermal conductivity in the
177 middle of the spin-crossover region above 2000 K. The effect of the spin crossover on
178 V_P decreases noticeably with increasing temperature (Fig. 1a), while the peak value of
179 R_{C_V} is approximately 1.15 at any temperature (Fig. 1b). Therefore, above a certain
180 temperature (~ 2000 K), the effect of increasing C_V almost cancels out that of the
181 decreasing V_P , and the spin crossover has a negligible effect on the thermal
182 conductivity in the middle of the spin-crossover region. The pressure region with the
183 negligible effect broadens with increasing temperature. Outside of the region, the spin
184 crossover reduces significantly the thermal conductivity. Thus, R_k fluctuates
185 significantly with pressure and temperature within the spin-crossover region. The
186 pressure regions with the thermal conductivity fluctuations broaden dramatically with
187 temperature (Fig. 3).

188 Therefore, the spin crossover can completely change the conventional
189 temperature and pressure relation of the thermal conductivity, even under CMB
190 conditions. In general, the lattice thermal conductivity increases with pressure and
191 decreases with temperature. The normal pressure dependence of the thermal
192 conductivity can be expressed as [*Hofmeister*, 1999]:

193
$$\frac{\partial \ln k_{latt}}{\partial P} = \frac{1}{K_T} \left(4\gamma + \frac{1}{3} \right) \quad (12)$$

194 where K_T is the isothermal bulk modulus and γ is the Grüneisen parameter. As
195 shown in Table 2, the unusual fluctuation in the thermal conductivity of ferropericlase
196 caused by the spin crossover can be compared to the normal pressure dependence of
197 the thermal conductivity. In fact, the normal pressure dependence of the thermal
198 conductivity at a relatively low temperature, as described by Eq. 12, is not sufficient
199 to balance the rapid decrease in the thermal conductivity caused by spin crossover
200 (Table 2). The thermal conductivity of ferropericlase will exhibit a double-valley
201 feature with increasing pressure at relative low temperature. A temperature of 1000 K
202 may be appropriate for the experimental observation of the double-valley feature. As
203 shown in Fig. 3, at room temperature, the two valleys are very close each other with a
204 3.5 GPa interval, which challenges the experimental observation. The distance
205 between valleys increase quickly with temperature (Table 1), while the double-valley
206 feature weakens with temperature (Table 2). Overall, 1000 K should be a good
207 choice.

208 The theoretical calculations [Stackhouse *et al.*, 2010; Tang and Dong, 2010]
209 predicted that the lattice thermal conductivity of pure simple cubic MgO at high
210 temperature follows the T^{-1} relation. The T dependence of the thermal conductivity for
211 $\text{Mg}_{1-x}\text{Fe}_x\text{O}$ becomes more gradual than T^{-1} because of the mass disorder introduced by
212 replacing Mg with Fe. Manthilake *et al.* [Manthilake *et al.*, 2011] found the $T^{0.24}$
213 dependence of the thermal conductivity of $\text{Mg}_{1-x}\text{Fe}_x\text{O}$ with $x=0.05$ and 0.2 at 8 and 14
214 GPa. As shown in Table 3 and Fig. 3c, the unusual fluctuation in the thermal
215 conductivity of ferropericlase caused by spin crossover can also be compared to the
216 normal T dependence of the thermal conductivity, and the spin crossover will
217 dramatically change the T dependence of the thermal conductivity of ferropericlase.
218 In some of the PT range, the positive T dependence of the thermal conductivity
219 produced by the spin crossover may cancel out the normal T dependence, and the
220 thermal conductivity of ferropericlase even increases with temperature, while in the
221 other part of the PT range, the thermal conductivity of ferropericlase decreases with T
222 much faster than the normal T dependence because of the spin-crossover effect (Fig. 2
223 and 3c). Thus, spin crossover generates a complicated T dependence of the thermal
224 conductivity of ferropericlase.

225 **Implications**

226 The spin crossover occurs not only in ferropericlase but also in bridgmanite and
227 post perovskite [Badro *et al.*, 2004; Lin *et al.*, 2013]. Iron can be Fe^{2+} and Fe^{3+} and
228 can occupy the Mg and Si sites in bridgmanite and post perovskite. The theoretical

229 and experimental studies indicate that only Fe³⁺ in the Si site experiences a high spin
230 to a low spin transition with a transition pressure at 15-50 GPa at 300 K [*Catalli et al.*,
231 2010; *Hsu et al.*, 2011; *Jackson et al.*, 2005; *Lin et al.*, 2012; *Stackhouse et al.*, 2007].
232 The spin transition in bridgmanite is also a smooth transition. The pressure range of
233 the spin crossover broadens with increasing temperature. The spin crossover causes a
234 significant softening in the bulk modulus of bridgmanite [*Shukla et al.*, 2016]. These
235 features are common in minerals with a spin crossover (e.g., [*Hsu*, 2017; *Y Wu et al.*,
236 2016]). Thus, the unusual effect of the spin crossover on the thermal conductivity of
237 ferropericlase should also apply to other minerals with a spin crossover such as
238 bridgmanite and post perovskite. In this study, the spin crossover significantly affects
239 the thermal conductivity of ferropericlase, even at the CMB conditions. The
240 bridgmanite and post perovskite have a similar transition pressure to ferropericlase at
241 room temperature. The recent experiments did not observe the spin transition effect
242 on thermal conductivity of bridgmanite at the lower-mantle pressure [*Hsieh et al.*,
243 2017; *Okuda et al.*, 2017], which is consistent with that the measured samples do not
244 contain iron in Si site. However, if there is a significant amount of Fe³⁺ in the Si sites
245 of bridgmanite and post perovskite, the spin crossover potentially dramatically
246 changes the thermal conductivity of the lower mantle at the CMB and affects our
247 estimation of the heat flow from the core to mantle.

248 Because of the unusual effect of the spin crossover on the thermal conductivity of
249 ferropericlase, the thermal conductivity of ferropericlase with a spin crossover no

250 longer complies with the conventional pressure and temperature dependence.
251 Considering the broad temperature and pressure range where the spin crossover
252 significantly affects the thermal conductivity (Fig. 2), we should be careful in
253 extrapolating the thermal conductivity of minerals with spin crossover to Earth's
254 interior conditions.

255 Spin crossover not only change the sound velocity and heat capacity but also
256 affect the mean free lifetime $\langle\tau\rangle$. $\langle\tau\rangle$ of MS may be smaller than the weight average
257 of that of LS and of HS because of increased scattering in MS with two types of iron.
258 Thus, R_k probably is reduced further after including the spin-crossover effect on $\langle\tau\rangle$.
259 This study combining with the effect of the spin crossover on the mean free lifetime
260 $\langle\tau\rangle$, which remains to be investigated in the future, will allow us to fully understand
261 the spin crossover effect on the thermal conductivity of ferroperricite.

262

263 **Acknowledgments**

264 The author thanks Renata M. Wentzcovitch for her constructive suggestions. This
265 work is financially supported by the Strategic Priority Research Program (B) of
266 Chinese Academy of Sciences, Grant No. XDB18000000, the Natural Science
267 Foundation of China (41721002), the Fundamental Research Funds for the Central
268 Universities (WK2080000078).

269

270

- 271 Badro, J., J. P. Rueff, G. Vanko, G. Monaco, G. Fiquet, and F. Guyot (2004),
272 Electronic transitions in perovskite: Possible nonconvecting layers in the lower
273 mantle, *Science*, 305(5682), 383-386.
- 274 Beck, P., A. F. Goncharov, V. V. Struzhkin, B. Militzer, H. K. Mao, and R. J. Hemley
275 (2007), Measurement of thermal diffusivity at high pressure using a transient
276 heating technique, *Applied Physics Letters*, 91(18). 181914
- 277 Bower, D. J., M. Gurnis, J. M. Jackson, and W. Sturhahn (2009), Enhanced
278 convection and fast plumes in the lower mantle induced by the spin transition in
279 ferropericlase, *Geophysical Research Letters*, 36. L10306
- 280 Catalli, K., S. H. Shim, V. B. Prakapenka, J. Y. Zhao, W. Sturhahn, P. Chow, Y. M.
281 Xiao, H. Z. Liu, H. Cynn, and W. J. Evans (2010), Spin state of ferric iron in
282 MgSiO₃ perovskite and its effect on elastic properties, *Earth and Planetary Science*
283 *Letters*, 289(1-2), 68-75.
- 284 Crowhurst, J. C., J. M. Brown, A. F. Goncharov, and S. D. Jacobsen (2008), Elasticity
285 of (Mg,Fe)O through the spin transition of iron in the lower mantle, *Science*,
286 319(5862), 451-453.
- 287 Dalton, D. A., W. P. Hsieh, G. T. Hohensee, D. G. Cahill, and A. F. Goncharov
288 (2013), Effect of mass disorder on the lattice thermal conductivity of MgO
289 periclase under pressure, *Scientific Reports*, 3, 2400.
- 290 de Koker, N. (2009), Thermal Conductivity of MgO Periclase from Equilibrium First
291 Principles Molecular Dynamics, *Physical Review Letters*, 103(12). 125902
- 292 de Koker, N. (2010), Thermal conductivity of MgO periclase at high pressure:
293 Implications for the D " region, *Earth and Planetary Science Letters*, 292(3-4),
294 392-398.
- 295 Dekura, H., T. Tsuchiya, and J. Tsuchiya (2013), Ab initio Lattice Thermal
296 Conductivity of MgSiO₃ Perovskite as Found in Earth's Lower Mantle, *Physical*
297 *Review Letters*, 110(2). 025904.
- 298 Fei, Y. W., L. Zhang, A. Corgne, H. Watson, A. Ricolleau, Y. Meng, and V.
299 Prakapenka (2007), Spin transition and equations of state of (Mg, Fe)O solid
300 solutions, *Geophysical Research Letters*, 34(17), L17307.
- 301 Ghaderi, N., D-B. Zhang, H. Zhang, J. Xian, R. M. Wentzcovitch, and T. Sun (2017),
302 Lattice Thermal Conductivity of MgSiO₃ Perovskite from First Principles,
303 *Scientific Reports*, 7, 5417
- 304 Goncharov, A. F., V. V. Struzhkin, J. A. Montoya, S. Kharlamova, R. Kundargi, J.
305 Siebert, J. Badro, D. Antonangeli, F. J. Ryerson, and W. Mao (2010), Effect of
306 composition, structure, and spin state on the thermal conductivity of the Earth's
307 lower mantle, *Physics of the Earth and Planetary Interiors*, 180(3-4), 148-153.
- 308 Haigis, V., M. Salanne, and S. Jahn (2012), Thermal conductivity of MgO, MgSiO₃
309 perovskite and post-perovskite in the Earth's deep mantle, *Earth and Planetary*
310 *Science Letters*, 355, 102-108.
- 311 Hofmeister, A. M. (1999), Mantle values of thermal conductivity and the geotherm
312 from phonon lifetimes, *Science*, 283(5408), 1699-1706.

- 313 Hofmeister, A. M. (2010), Thermal diffusivity of oxide perovskite compounds at
314 elevated temperature, *Journal of Applied Physics*, 107(10). 103532.
- 315 Hofmeister, A. M. (2014), Thermal diffusivity and thermal conductivity of
316 single-crystal MgO and Al₂O₃ and related compounds as a function of temperature,
317 *Physics and Chemistry of Minerals*, 41(5), 361-371.
- 318 Hofmeister, A. M. and Branlund, J. M. (2015), Thermal Conductivity of the Earth,
319 in *Treatise on Geophysics*, 2nd edition, Volume 2, 584-608.
- 320 Hsieh W-P, Deschamps F, Okuchi T, Lin J-F (2017) Reduced lattice thermal
321 conductivity of Fe-bearing bridgmanite in Earth's deep mantle. *J Geophys Res*
322 *Solid Earth* 122: 4900–4917.
- 323 Hsieh W-P, Deschamps F, Okuchi T, Lin J-F (2018) Effects of iron on the lattice
324 thermal conductivity of Earth's deep mantle and implications for mantle dynamics,
325 *Proceedings of the National Academy of Sciences of the United States of*
326 *America*, <https://doi.org/10.1073/pnas.1718557115>
- 327 Hsu, H. (2017), First-principles study of iron spin crossover in the new hexagonal
328 aluminous phase, *Physical Review B*, 95(2), 020406.
- 329 Hsu, H., P. Blaha, M. Cococcioni, and R. M. Wentzcovitch (2011), Spin-State
330 Crossover and Hyperfine Interactions of Ferric Iron in MgSiO₃ Perovskite,
331 *Physical Review Letters*, 106(11), 118501.
- 332 Huang, C., W. Leng, and Z. Q. Wu (2015), Iron-spin transition controls structure and
333 stability of LLSVPs in the lower mantle, *Earth and Planetary Science Letters*, 423,
334 173-181.
- 335 Imada, S., K. Ohta, T. Yagi, K. Hirose, H. Yoshida, and H. Nagahara (2014),
336 Measurements of lattice thermal conductivity of MgO to core-mantle boundary
337 pressures, *Geophysical Research Letters*, 41(13), 4542-4547.
- 338 Jackson, J. M., W. Sturhahn, G. Y. Shen, J. Y. Zhao, M. Y. Hu, D. Errandonea, J. D.
339 Bass, and Y. W. Fei (2005), A synchrotron Mossbauer spectroscopy study of
340 (Mg,Fe)SiO₃ perovskite up to 120 GPa, *American Mineralogist*, 90(1), 199-205.
- 341 Katsura, T. (1997), Thermal diffusivity of periclase at high temperatures and high
342 pressures, *Physics of the Earth and Planetary Interiors*, 101(1-2), 73-77.
- 343 Komabayashi, T., K. Hirose, Y. Nagaya, E. Sugimura, and Y. Ohishi (2010),
344 High-temperature compression of ferropericlase and the effect of temperature on
345 iron spin transition, *Earth and Planetary Science Letters*, 297(3-4), 691-699.
- 346 Lin, J. F., and T. Tsuchiya (2008), Spin transition of iron in the Earth's lower mantle,
347 *Physics of the Earth and Planetary Interiors*, 170(3-4), 248-259.
- 348 Lin, J. F., S. Speziale, Z. Mao, and H. Marquardt (2013), Effects of the Electronic
349 Spin Transitions of Iron in Lower Mantle Minerals: Implications for Deep Mantle
350 Geophysics and Geochemistry, *Reviews of Geophysics*, 51(2), 244-275.
- 351 Lin, J. F., E. E. Alp, Z. Mao, T. Inoue, C. McCammon, Y. M. Xia, P. Chow, and J. Y.
352 Zhao (2012), Electronic spin states of ferric and ferrous iron in the lower-mantle
353 silicate perovskite, *American Mineralogist*, 97(4), 592-597.

- 354 Manga, M., and R. Jeanloz (1997), Thermal conductivity of corundum and periclase
355 and implications for the lower mantle, *Journal of Geophysical Research-Solid*
356 *Earth*, 102(B2), 2999-3008.
- 357 Manthilake, G. M., N. de Koker, D. J. Frost, and C. A. McCammon (2011), Lattice
358 thermal conductivity of lower mantle minerals and heat flux from Earth's core,
359 *Proceedings of the National Academy of Sciences of the United States of America*,
360 108(44), 17901-17904.
- 361 Mao, Z., J. F. Lin, J. Liu, and V. B. Prakapenka (2011), Thermal equation of state of
362 lower-mantle ferropericlase across the spin crossover, *Geophysical Research*
363 *Letters* 38, L23308.
- 364 Marquardt, H., S. Speziale, H. J. Reichmann, D. J. Frost, F. R. Schilling, and E. J.
365 Garnero (2009), Elastic Shear Anisotropy of Ferropericlase in Earth's Lower
366 Mantle, *Science*, 324(5924), 224-226.
- 367 Ohta, K., T. Yagi, and K. Hirose (2014), Thermal diffusivities of MgSiO₃ and
368 Al-bearing MgSiO₃ perovskites, *American Mineralogist*, 99(1), 94-97.
- 369 Ohta, K., T. Yagi, K. Hirose, and Y. Ohishi (2017), Thermal conductivity of
370 ferropericlase in the Earth's lower mantle, *Earth and Planetary Science Letters*, 465,
371 29-37.
- 372 Osako, M., and E. Ito (1991), Thermal-Diffusivity of MgSiO₃ Perovskite, *Geophysical*
373 *Research Letters*, 18(2), 239-242.
- 374 Persson, K., A. Bengtson, G. Ceder, and D. Morgan (2006), Ab initio study of the
375 composition dependence of the pressure-induced spin transition in the
376 (Mg_{1-x},Fe_x)O system, *Geophysical Research Letters*, 33(16), L16306.
- 377 Rainey, E. S. G., and A. Kavner (2014), Peak scaling method to measure temperatures
378 in the laser-heated diamond anvil cell and application to the thermal conductivity
379 of MgO, *Journal of Geophysical Research-Solid Earth*, 119(11), 8154-8170.
- 380 Shahnas, M. H., and W. R. Peltier (2015), The impacts of mantle phase transitions
381 and the iron spin crossover in ferropericlase on convective mixing: the evidence
382 for compositional convection definitive? New results from a Yin-Yang overset
383 grid-based control volume model, *Journal of Geophysical Research-Solid Earth*,
384 120(8), 5884-5910.
- 385 Shahnas, M. H., R. N. Pysklywec, and D. A. Yuen (2016), Spawning superplumes
386 from the midmantle: The impact of spin transitions in the mantle, *Geochemistry*
387 *Geophysics Geosystems*, 17(10), 4051-4063.
- 388 Shahnas, M. H., D. A. Yuen, and R. N. Pysklywec (2017), Mid-mantle
389 heterogeneities and iron spin transition in the lower mantle: Implications for
390 mid-mantle slab stagnation, *Earth and Planetary Science Letters*, 458, 293-304.
- 391 Shahnas, M. H., W. R. Peltier, Z. Wu, and R. Wentzcovitch (2011), The high-pressure
392 electronic spin transition in iron: Potential impacts upon mantle mixing, *Journal of*
393 *Geophysical Research-Solid Earth*, 116, B08205.

- 394 Shukla, G., M. Cococcioni, and R. M. Wentzcovitch (2016), Thermoelasticity of
395 Fe³⁺- and Al-bearing bridgmanite: Effects of iron spin crossover, *Geophysical*
396 *Research Letters*, 43(11), 5661-5670.
- 397 Stackhouse, S., J. P. Brodholt, and G. D. Price (2007), Electronic spin transitions in
398 iron-bearing MgSiO₃ perovskite, *Earth and Planetary Science Letters*, 253(1-2),
399 282-290.
- 400 Stackhouse, S., L. Stixrude, and B. B. Karki (2010), Thermal Conductivity of
401 Periclase (MgO) from First Principles, *Physical Review Letters*, 104(20), 208501.
- 402 Stackhouse, S., L. Stixrude, and B. B. Karki (2015), First-principles calculations of
403 the lattice thermal conductivity of the lower mantle, *Earth and Planetary Science*
404 *Letters*, 427, 11-17.
- 405 Tang, X. L., and J. J. Dong (2010), Lattice thermal conductivity of MgO at conditions
406 of Earth's interior, *Proceedings of the National Academy of Sciences of the United*
407 *States of America*, 107(10), 4539-4543.
- 408 Tang, X. L., M. C. Ntam, J. J. Dong, E. S. G. Rainey, and A. Kavner (2014), The
409 thermal conductivity of Earth's lower mantle, *Geophysical Research Letters*, 41(8),
410 2746-2752.
- 411 Tsuchiya, T., R. M. Wentzcovitch, C. R. S. da Silva, and S. de Gironcoli (2006), Spin
412 transition in magnesiowustite in earth's lower mantle, *Physical Review Letters*,
413 96(19), 198501.
- 414 van der Hilst, R. D., and H. Karason (1999), Compositional heterogeneity in the
415 bottom 1000 kilometers of Earth's mantle: Toward a hybrid convection model,
416 *Science*, 283(5409), 1885-1888.
- 417 Wentzcovitch, R. M., J. F. Justo, Z. Wu, C. R. S. da Silva, D. A. Yuen, and D.
418 Kohlstedt (2009), Anomalous compressibility of ferropericlase throughout the iron
419 spin cross-over, *Proceedings of the National Academy of Sciences of the United*
420 *States of America*, 106(21), 8447-8452.
- 421 Wu, and Wentzcovitch (2014), Spin crossover in ferropericlase and velocity
422 heterogeneities in the lower mantle. *Proceedings of the National Academy of*
423 *Sciences of the United States of America*, 111(29), 10468-10472.
- 424 Wu, Y., X. Wu, J. F. Lin, C. A. McCammon, Y. M. Xiao, P. Chow, V. B. Prakapenka,
425 T. Yoshino, S. M. Zhai, and S. Qin (2016), Spin transition of ferric iron in the NAL
426 phase: Implications for the seismic heterogeneities of subducted slabs in the lower
427 mantle, *Earth and Planetary Science Letters*, 434, 91-100.
- 428 Wu, Z., J. F. Justo, C. R. S. da Silva, S. de Gironcoli, and R. M. Wentzcovitch (2009),
429 Anomalous thermodynamic properties in ferropericlase throughout its spin
430 crossover transition, *Physical Review B*, 80(1), 014409.
- 431 Wu, Z. Q. (2016), Velocity structure and composition of the lower mantle with spin
432 crossover in ferropericlase, *Journal of Geophysical Research-Solid Earth*, 121(4),
433 2304-2314.

- 434 Wu, Z. Q., and R. M. Wentzcovitch (2017), Composition versus temperature induced
435 velocity heterogeneities in a pyrolitic lower mantle, *Earth and Planetary Science*
436 *Letters*, 457, 359-365.
- 437 Wu, Z.Q., J. F. Justo, C.R.S. da Silva, S. de Gironcoli, R. M. Wentzcovitch (2009).
438 Anomalous thermodynamic properties in ferropericlase throughout its
439 spin crossover transition. *Physical Review B*, 80, 014409.
- 440 Wu, Z. Q., J. F. Justo, and R. M. Wentzcovitch (2013), Elastic Anomalies in a
441 Spin-Crossover System: Ferropericlase at Lower Mantle Conditions, *Physical*
442 *Review Letters*, 110(22), 228501.
- 443 Yang, J., X. Y. Tong, J. F. Lin, T. Okuchi, and N. Tomioka (2015), Elasticity of
444 Ferropericlase across the Spin Crossover in the Earth's Lower Mantle, *Scientific*
445 *Reports*, 5, 17188.
- 446 Zhang, D-B., P. B. Allen, T. Sun, and R. M. Wentzcovitch (2017), Thermal
447 conductivity from phonon quasiparticles with subminimal mean free path in
448 the MgSiO₃ perovskite, *Physical review B*, 96, 100302.
- 449 Zhao, D. P. (2007), Seismic images under 60 hotspots: Search for mantle plumes,
450 *Gondwana Research*, 12(4), 335-355.
- 451
452
453

454

455 **Table 1.** The valley/peak values of R_k and the corresponding pressure that they occur
456 for ferropericalse with $X_{Fe}=0.1875$. The number in parentheses is the pressure
457 variation required to change R_k 5%

T (K)	Valley 1		Peak		Valley 2	
	value	P (GPa)	value	P (GPa)	value	P (GPa)
300	0.59	38 (0.8)	0.66	40.5 (1.0)	0.65	41.5 (1.1)
1000	0.74	47.5 (2.0)	0.83	54.5 (3.5)	0.80	60 (4.5)
2000	0.81	60 (6.0)	0.92	74 (7.5)	0.85	89 (11)
3000	0.84	72 (9.0)	0.95	93.5 (12)	0.87	118.5 (17)
4000	0.86	84.5 (13.5)	0.97	114.5 (16)	0.88	148.5 (19)

458

459

460

461 **Table 2.** The maximum and minimum of the pressure dependence of R_k at various
 462 temperatures and the corresponding pressure for ferropicalse with $X_{Fe}=0.1875$.
 463 $\frac{\partial \ln k_{latt}}{\partial P}$ for high spin state in the last row is calculated with Eq. 12 at pressure and
 464 temperature of $(\partial R_k / \partial P)_{\min}$. The number in parentheses is the pressure variation
 465 required to change $\partial R_k / \partial P$ 10%

T (K)		300	1000	2000	3000	4000
$(\partial R_k / \partial P)_{\min}$	value ($10^{-2}/\text{GPa}$)	-12	-2.9	-1.1	-0.7	-0.5
	P (GPa)	36 (0.2)	42 (0.6)	51.5 (0.9)	61 (1.1)	70.5 (1.4)
$(\partial R_k / \partial P)_{\max}$	value ($10^{-2}/\text{GPa}$)	7.7	2.1	1.2	0.9	0.6
	P (GPa)	44 (0.4)	50 (0.5)	66 (0.8)	82 (1.1)	99 (1.5)
$(\partial \ln k_{latt} / \partial P)$ ($10^{-2}/\text{GPa}$)		1.88	1.89	1.83	1.75	1.7

466
 467
 468

469 **Table 3.** The maximum and minimum of the temperature dependence of R_k at various
 470 pressures for ferropericlase with $X_{Fe}=0.1875$. The last row shows $\frac{\partial \ln k_{latt}}{\partial T}$ for $T^{0.24}$
 471 dependence of thermal conductivity at pressure and temperature of $(\partial R_k / \partial T)_{max}$. The
 472 number in parentheses is the temperature variation required to change $\partial R_k / \partial T$ 10%.

P (GPa)		<32	40	80	100	136
$(\partial R_k / \partial T)_{min}$	Value ($10^{-4}/K$)	0	-6.5	-3	-1.8	-1.1
	T (K)		360 (10)	1300 (40)	1800 (50)	2800 (80)
$(\partial R_k / \partial T)_{max}$	Value ($10^{-4}/K$)	0	7	2.0	1.5	1.2
	T (K)		600 (20)	1980 (30)	2800 (50)	4050 (70)
$\frac{\partial \ln k_{latt}}{\partial T} (= -0.24/T)$			-4	-1.21	-0.86	-0.59

473
 474
 475
 476
 477
 478

479 **Figure caption**

480 **Figure 1.** (a) V_P / V_P^{mix} and (b) C_V / C_V^{mix} for ferropericalse with $X_{Fe}=0.1875$ as
481 function of temperature and pressure.

482 **Figure 2.** k / k^{mix} as function of temperature and pressure for ferropericalse with
483 $X_{Fe}=0.1875$.

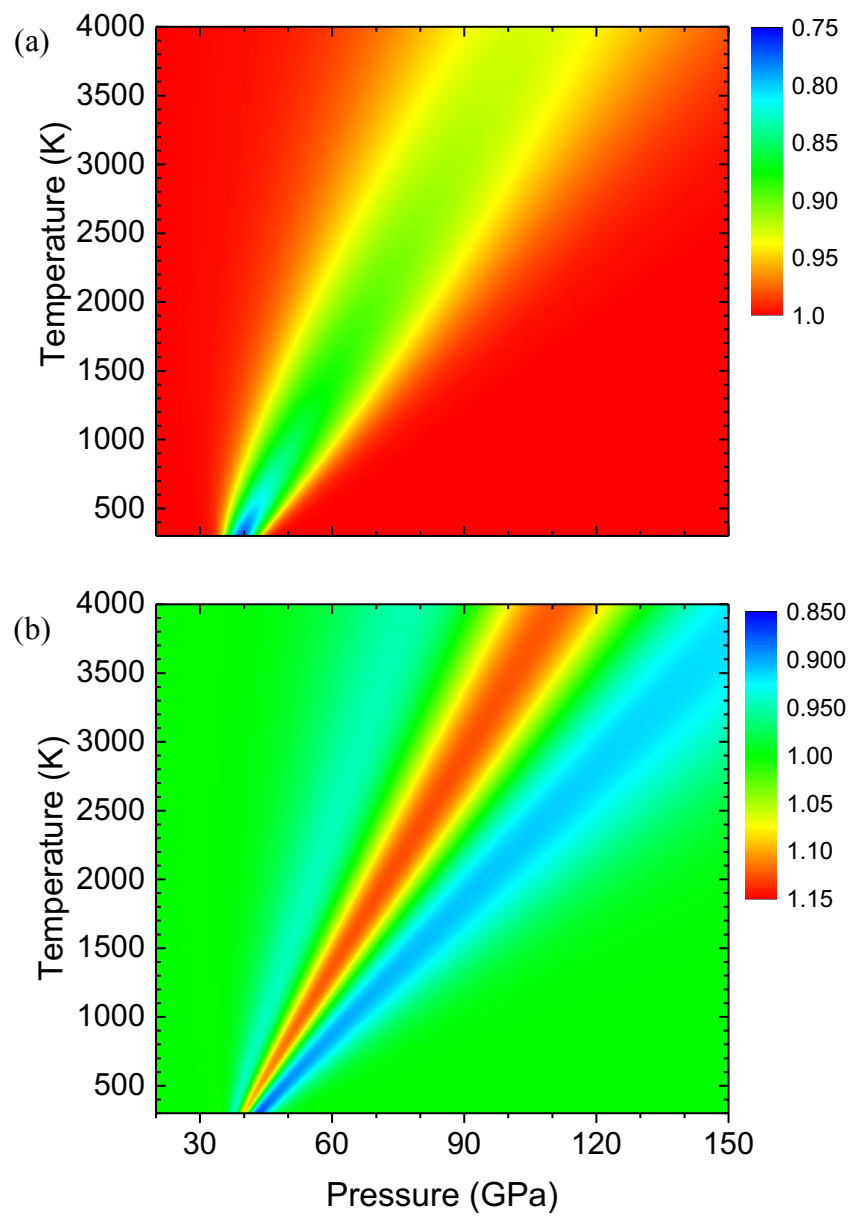
484 **Figure 3.** (a) pressure dependence of k / k^{mix} at various temperatures for
485 ferropericalse with $X_{Fe}=0.1875$. (b) the pressure dependence of k at room temperature
486 measured by Ohta et al (2017). The dashed line in (a) describes the ratio of the solid
487 green line over the dashed green line in (b). and (c) the temperature dependence of
488 k / k^{mix} at various pressures

489

490

491

492

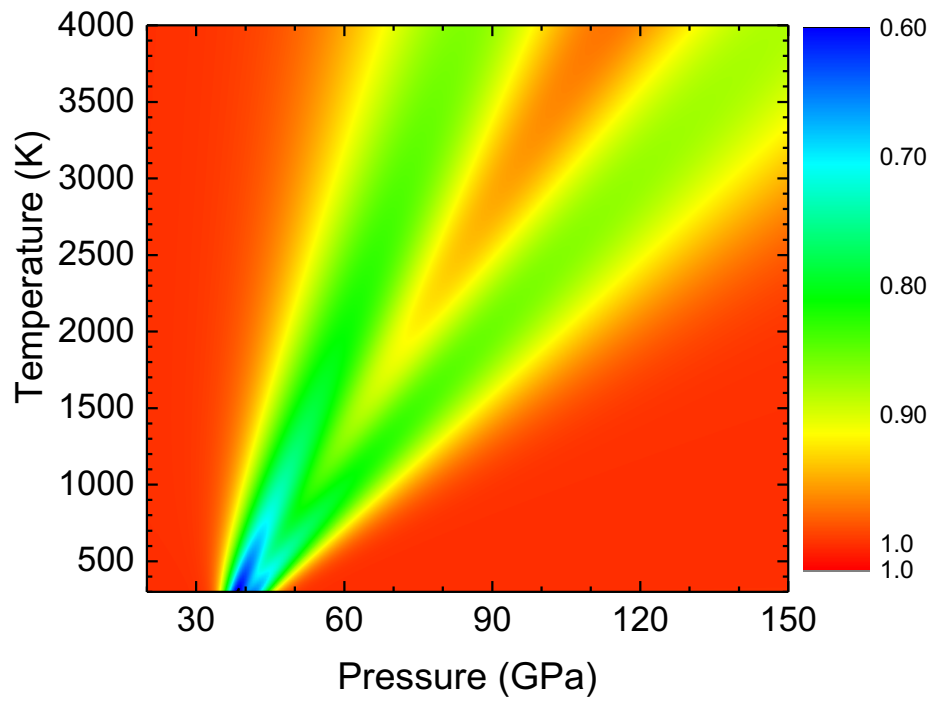


493

494

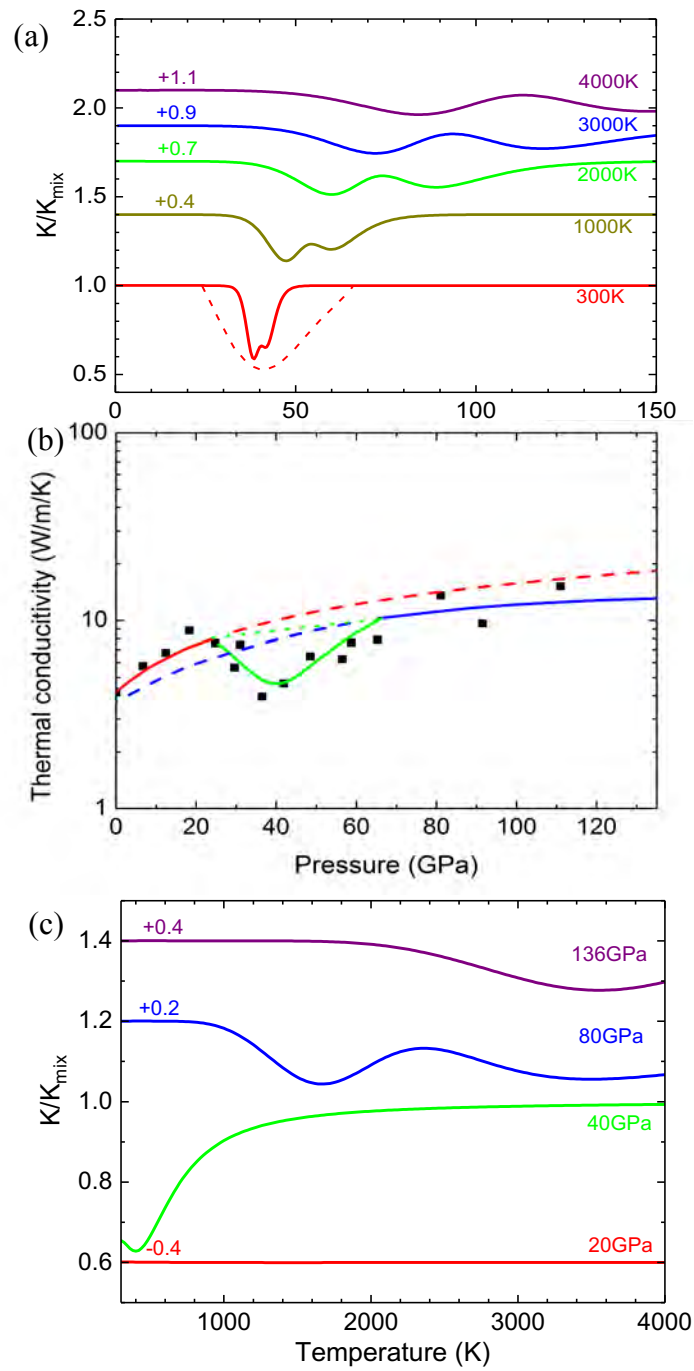
495

496 **Figure 1**



497
498
499
500
501
502
503
504
505
506
507
508

Figure 2



509
510
511
512
513

Figure 3